Kinetics and Mechanisms for the Cylinder-to-Gyroid Transition in a Block Copolymer Solution

Chia-Ying Wang† and Timothy P. Lodge*

Department of Chemistry and Department of Chemical Engineering & Materials Science, University of Minnesota, Minneapolis, Minnesota 55455-0431

Received April 1, 2002

ABSTRACT: The cylinder-to-gyroid transition in a block copolymer solution has been studied using a combination of rheology and small-angle X-ray scattering (SAXS). A poly(styrene-*b*-isoprene) diblock copolymer with block molecular weights of 11 000 and 32 000 g/mol, respectively, dissolved in the styrene-selective solvent di-*n*-butyl phthalate (DBP) at a volume fraction of 0.67 exhibits an order−order transition between hexagonally packed cylinders (C) and the cubic gyroid phase (G) at 74 ± 3 °C. A shear-oriented C phase transforms to G epitaxially, as previously established in melts. For shallow quenches into G, the transition proceeds directly by a nucleation and growth process. For deeper quenches, a metastable intermediate structure appears, with scattering and rheological features consistent with the hexagonally perforated layer (HPL) state. The appearance of the HPL state beyond a certain quench depth is reconciled with previous experiments and theory for the lamellar (L)-to-gyroid transition. The C → G transition follows the same pathways, and at approximately the same rates, even when the initial C phase is not shear-oriented. The transition rates are quantified as a function of quench depth. The reverse G → C transition demonstrates a memory of the initial cylinder orientation that persists even after annealing the G phase for 48 h. The results are discussed and compared with related work in the literature.

Introduction

Self-assembled block copolymers display a rich variety of thermoreversible order−order phase transitions (OOTs) between states of different symmetry.[1,2] The structural length scales are amenable to study by small-angle scattering (SAXS and SANS), and the typically slow kinetics (i.e., seconds to days) allow for detailed examination of the transition pathways. In some cases it is even possible to capture transient or metastable intermediate states for examination by, for example, electron microscopy. Mean-field theory has proven to be very successful in calculating the relative free energies of the various morphologies and has recently been extended to consider transition mechanisms.[3−9] For diblock copolymers in the melt, the established equilibrium ordered phases are lamellae (L), hexagonally packed cylinders (C), the gyroid (G), and a body-centered-cubic (bcc) array of spheres (S). The relevant OOTs are C ↔ S,[10−19] L ↔ C,[20−22] L ↔ G,[23−26] and C ↔ G.[27−30] In all cases epitaxial relationships have been established between the initial and final states. This step has been greatly facilitated by shear orientation of the initial structure, which enables a more definitive assignment of Bragg reflections in small-angle scattering. The transition kinetics and detailed mechanisms are not yet so well understood, however. Among the interesting issues are the following: (i) Do OOTs proceed by nucleation and growth, or do spinodal boundaries play a role? (ii) Do the kinetics and pathways depend on the preorientation of the initial state? (iii) For which transitions do metastable intermediates appear? In this paper we examine the C → G transition in a block copolymer solution, as a function of the depth of the temperature quench into the final state and as a function of the preorientation of the cylinders, and discuss the results in terms of these issues.

We have recently conducted a broad study of the phase behavior of poly(styrene-*b*-isoprene) diblock copolymers in solvents of varying selectivity.[31−34] This work has suggested that block copolymer solutions may possess some advantages over melts in terms of studying OOTS. The use of solvents of differing selectivity, and the temperature dependence of the selectivity, can provide access to several different OOTs for a single polymer. Adjustment of concentration, molecular weight, and selectivity can be used to place the transition in a "kinetically convenient" regime, e.g., closer to or further from the glass transition according to whether the kinetics are otherwise too fast or too slow. Also, new phases can be accessed in solution, such as a face-centered-cubic (fcc) or hexagonally close-packed (hcp) array of spheres; we have recently demonstrated epitaxial relationships between fcc/hcp and bcc micellar packings.[35] The phase behavior of the particular copolymer employed herein in the styrene-selective solvent di-*n*-butyl phthalate (DBP) has been reported.[33,34] For solutions with copolymer volume fraction near 0.67, the following series of equilibrium phases was observed upon heating: L → G → C → disorder. In the first set of experiments reported here, large-amplitude shear deformation at elevated temperatures was used to prepare oriented cylinders (o-C). Then, rheology and SAXS were used to follow the o-C → G transition following various temperature quenches across the transition, $T_{OOT} = 74 \pm 3$ °C. A preliminary account of these measurements has been given, focusing on the observation of an unexpected intermediate state prior to the formation of G following deep quenches.[30] In the second set of experiments, similar temperature jump experiments were performed, but originating from randomly oriented cylinders (ran-C). The kinetics and mechanisms of the two transitions (o-C → G and ran-C → G) are compared,

† Current address: Polymers Division, NIST, Gaithersburg, MD 20899.

* Author for correspondence: e-mail lodge@chem.umn.edu.

10.1021/ma0205212 CCC: $22.00
Published on Web 07/24/2002

and similarities and differences with related studies are discussed.

Experimental Section

Materials. A poly(styrene-*b*-isoprene) diblock copolymer, denoted SI(11−32), with block molecular weights of 1.1×10^4 and 3.2×10^4 g/mol, respectively, was synthesized via living anionic polymerization using standard procedures.[32] The number-average block molecular weight and the polydispersity index, M_w/M_n, of 1.02 were determined using size-exclusion chromatography, and the composition was determined by ^{1}H NMR. The styrene-selective solvent, di-*n*-butyl phthalate (DBP), was purchased from Aldrich and purified by distillation at 150 °C under vacuum. The solutions were prepared gravimetrically by adding both SI(11−32) and DBP into the cosolvent methylene chloride. The cosolvent was then evaporated under a stream of nitrogen at room temperature until constant weight was achieved. Based on additivity of volumes and densities for SI(11−32) and DBP of 0.944 and 1.043 g/mL, respectively, the volume fraction of copolymer (ϕ) was calculated to be 0.67.

Order−Order Transition Temperatures. The phase diagram for SI(11−32) dissolved in the styrene-selective solvent DBP has been established previously.[33,34] As noted above, the following sequence of phases was determined for solutions with ϕ near 0.67: L → G → C → disorder. The order−order transition temperatures, T_{OOT}, were reconfirmed by rheological measurements using a Rheometrics dynamic mechanical thermal analyzer (DMTA). Samples were sandwiched between 12.5 mm diameter parallel plates with a gap width of 1 mm. The elastic modulus, G', and the loss modulus, G'', at a strain amplitude $\gamma = 1\%$ and frequency $\omega = 1$ rad/s were measured while scanning across the phase transition at various heating or cooling rates. The hysteresis, the difference between the transformation temperature of C → G by cooling and that of G → C upon heating, increased from ∼13 to ∼36 °C for scanning rates ($\partial T/\partial t$) ranging from 0.1 to 5 °C/min. Figure 1a shows the elastic modulus upon heating and cooling across the transition at several different rates. The transition temperature was taken as the midpoint of the rise/fall in G'. By extrapolating to the limit of zero scanning rate, T_{OOT}(G ↔ C) was determined to be 74 ± 3 °C, as illustrated in Figure 1b. A similar protocol located the other T_{OOT} at 48 ± 3 °C (L ↔ G) and the order−disorder temperature, T_{ODT}, as 122 ± 3 °C.

Rheology. Dynamic viscoelastic measurements were performed on the DMTA rheometer with sample thickness ranging from 0.3 to 1 mm. To study the transition from a well-oriented cylinder phase, o-C, the cylinders were shear-aligned at 85 °C, by applying $\gamma = 50\%$ and $\omega = 0.5$ rad/s for 1 h. Following different temperature quenches G' ($\gamma = 1\%$, $\omega = 1$ rad/s) was recorded vs time as the sample was annealed at the final temperature (from 58 to 71 °C) in the G window. These experimental protocols are illustrated in Figure 2. Typical quench times were less than 5 min, and time "zero" was taken to be when the rheometer was within ±0.5 °C of the destination temperature.

Similar temperature jump experiments were conducted to investigate the transition from randomly oriented cylinders (ran-C) to G. Solution samples were first held at 130 °C for 30 min in the disordered state and then quenched and annealed for 30 min at 85 °C, forming ran-C (as confirmed by SAXS). Following various temperature quenches (final temperatures from 60 to 71 °C), the time evolution of G' was monitored through the ran-C → G transition (see Figure 2).

Small-Angle X-ray Scattering (SAXS). An in-situ rheology and SAXS technique was employed to study the transition of o-C → G. The DMTA rheometer was installed on the University of Minnesota 6m SAXS line. The shear plates (12.5 mm × 12.5 mm) were modified with 3 mm diameter apertures machined into the center and covered by 50 μm Kapton films, to allow for transmission of the X-ray beam. Cu Kα X-rays, wavelength $\lambda = 1.54$ Å, are generated by a Rigaku RU-200BVH rotating anode equipped with a 0.2 × 2 mm microfocus

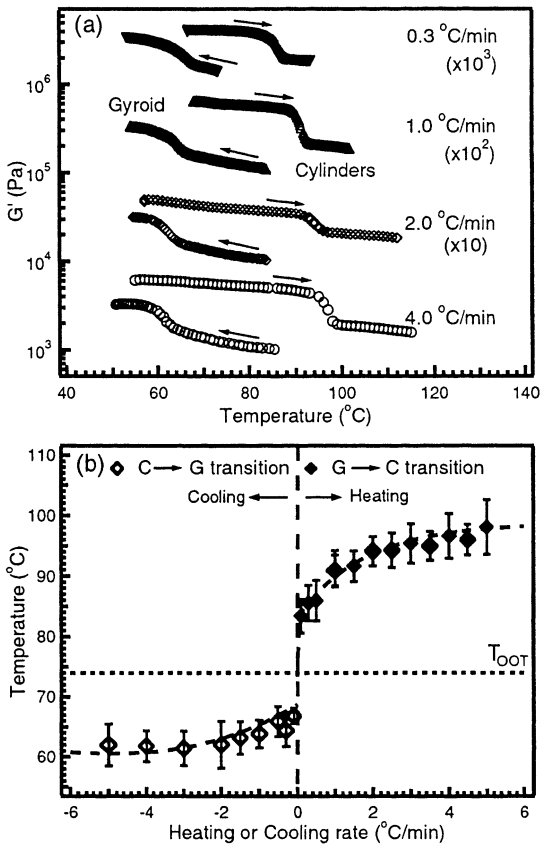

Figure 1. (a) G' for C → G and G → C at various heating and cooling rates; curves shifted vertically for clarity. (b) Transition temperatures at various heating and cooling rates.

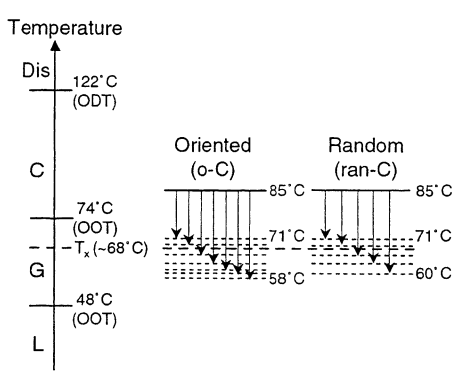

Figure 2. Map of the various temperature quenches employed.

cathode. Appropriate holes were also drilled through the DMTA temperature control jacket to permit X-ray transmission. Two-dimensional scattering patterns were collected for intervals of 300 s by an area detector (Siemens) and were corrected for the nonuniformity and spatial distortion of the detector. The sample−detector distance was 2.3 m, and the scattering vector q ranged from 0.007 to 0.09 Å^{-1},where $q = 4\pi \sin(\theta/2)/\lambda$ and θ is the scattering angle.

A highly oriented cylinder phase was prepared in situ at 90 °C, by applying $\gamma = 100\%$ and $\omega = 0.5$ rad/s for 2 h. The shear direction (z) was vertical, while the gradient (y) and the neutral directions (x) were horizontal. The X-ray beam was incident along y. The time evolution of the SAXS 2D patterns in the $x-z$ plane was monitored following various quenches from 90 °C (o-C) to G (60−69 °C). The experimental procedures are similar to those sketched in Figure 2, except that the initial cylinder phase was prepared at a slightly higher temperature, 90 °C.

A second SAXS line, operated with a thermostated sample chamber, was used to study the ran-C → G transition.

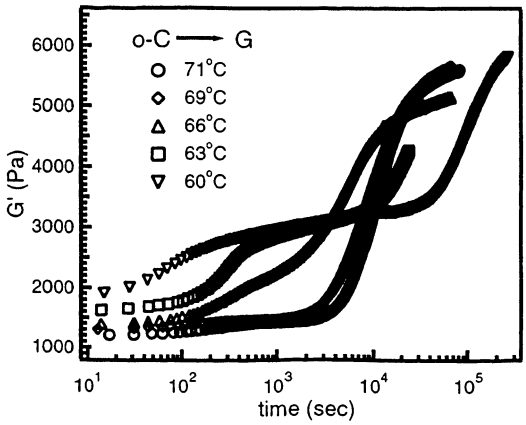

Figure 3. Evolution of G' ($\gamma = 1\%$ and $\omega = 1$ rad/s) following quenches from o-C to the indicated temperatures.

Solutions were sealed in 1.5 or 2 mm diameter quartz capillary tubes with high temperature silicone adhesive. Sample temperatures were controlled by a water/ethylene glycol cooled, electrically heated brass block, under a slight positive helium pressure within the closed sample chamber. Two-dimensional scattering patterns were collected for 1200 s intervals by the area detector at the end of a 2.4 m evacuated flight tube and were corrected for the nonlinear response of the detector. These imagines were azimuthally averaged to produce one-dimensional profiles of intensity, I, vs q. As in the rheological measurements, ran-C was obtained by quenching the sample from the disordered state at 130 °C and annealing for 30 min at 85 °C. The SAXS patterns were monitored with time following various temperature quenches from ran-C into G (60−69 °C).

Results and Discussion

We first examine the o-C → G transition by comparing the time evolution of G' and the SAXS patterns. An intermediate state appears for deep quenches but not for shallow quenches, and the epitaxial relationships of these transformation processes are discussed. A similar comparison between rheological measurements and SAXS is then presented for the ran-C → G transition. The transition mechanisms for ran-C → G are apparently similar to those observed for o−C → G, and accordingly, a common transition scenario is proposed. The transition kinetics are evaluated on the basis of the time evolution of G' at various quench temperatures, for both o-C → G and ran-C → C transitions. Finally, the reverse G → C transition is discussed briefly.

The o-C → G Transition. Following a temperature quench from the disordered state, arrays of hexagonally packed cylinders were formed with random orientations. These unoriented cylinders were shear-aligned to a significant degree at 85 °C, as evidenced by a considerable reduction in G' at low frequency (0.5 rad/s) and later confirmed by the in-situ rheology and SAXS measurements. The low-frequency behavior of ran-C is expected to be more solidlike than o-C, as the cylinders are less easily sheared along the alignment axis.[14] The o-C phase was then quenched to various lower temperatures. The transformation from o-C to G was monitored with time, as G exhibits a significantly greater elastic modulus due to its connectivity and cubic symmetry. Figure 3 displays the time evolution of G' following five temperature quenches. When the final temperature (71 and 69 °C) is close to T_{OOT} between C and G (74 °C), $\Delta T = |T - T_{OOT}| = 3$ or 5 °C, G' increases with time in one step. After a long induction period of approximately

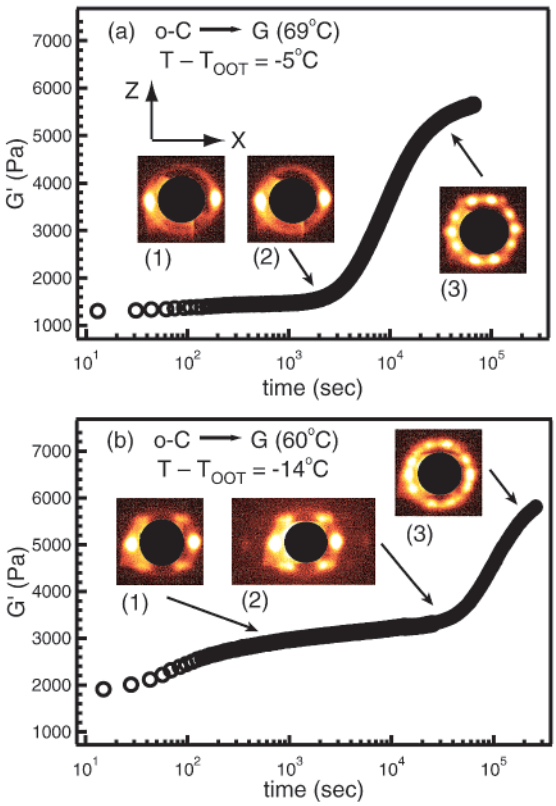

Figure 4. Evolution of G' compared to the corresponding SAXS patterns for (a) a "shallow" quench and (b) a "deep" quench from o-C.

3×10^3 s, G' increases sharply to a plateau after ca. 10^5 s. In contrast, after a deeper quench to 66 °C ($\Delta T = 8$ °C), G' increased in two distinct steps, where the second step began at roughly 400 s. The two distinct steps were even more clearly resolved when the o-C phase was quenched to a final temperature of 63 or 60 °C ($\Delta T = 11$ or 14 °C). In this case, the first process was largely completed within 10^3 s, whereas the sharp increase in G' for the second stage did not begin until after 10^4 s. It should be noted that in these instances G' did not achieve a second plateau at long annealing times (up to 3 days); rather, G' continued to increase slowly. Also, it should be noted that the quench depth is limited by the transition boundary between G and L phases (48 °C), and thus the maximum ΔT is 26 °C. The lowest quench temperature employed here was 58 °C ($\Delta T = 16$ °C, not shown), due to the slow kinetics.

The o-C → G transition was further studied by applying the in-situ SAXS and rheology technique. A highly oriented cylinder phase was attained at 90 °C by shear alignment, and SAXS measurements were conducted to study the microphase transformation from o-C to G. The 2D scattering pattern of the well-oriented cylinder phase displays two bright spots on the equator, as represented in pattern (1) in Figure 4a. These equatorial spots can be assigned as reflections from (10) hexagonal lattice planes, indicating that the cylinders are predominantly oriented along the shear direction z. The 2D SAXS images were averaged radially within an annulus of $q^* \pm 0.1q^*$, where q^* is the peak wave vector. Examples of the resulting 1D profile of intensity vs azimuthal angle, Φ, can be found in the previous report.[30] The azimuthal angle dependence of SAXS intensity, $I(\Phi)$, with the azimuthal angle of the peak designated as $\Phi = 0°$, was then utilized to estimate the

normalized orientation distribution function $f(\alpha)$:[36]

$$f(\alpha)\sin\alpha\,d\alpha = \frac{\sin\alpha\,d\alpha\int_{q_1}^{q_2} I(q,\alpha)q^2\,dq}{\int_0^{\pi}\sin\alpha\,d\alpha\int_{q_1}^{q_2} I(q,\alpha)q^2\,dq} \quad (1)$$

where q_1 and q_2 are the lower and upper bounds and are selected as $0.9q^*$ and $1.1q^*$, respectively, and α is the angle between the cylinder axis and the z axis (shear direction). The order parameter S was next calculated as[37]

$$S \equiv (3\langle\cos^2\alpha\rangle - 1)/2 \quad (2)$$

and

$$\langle\cos^2\alpha\rangle = \int_0^{\pi} f(\alpha)\cos^2\alpha\sin\alpha\,d\alpha \quad (3)$$

S ranges from 0 to 1 for totally random orientation to perfect alignment (all the cylinders are parallel to the shear direction). The order parameter was estimated to be 0.5 for pattern 1 in Figure 4a, indicating a fairly good alignment of the cylinders. Similar degrees of orientation, $S \approx 0.5$, were achieved for all the shear alignment of o-C in this work.

Following the temperature quench to 69 °C from o-C, the scattering pattern does not show any discernible change even 40 min after the rheometer reaches temperature equilibrium (pattern (2) in Figure 4a), indicating an induction period. The 10-spot scattering pattern characteristic of G (discussed below)[28,38] then appears rather abruptly, approximately at the same time as G' begins to rise. The 10-spot profile continues to sharpen and intensify with time, as illustrated by pattern (3) in Figure 4a, obtained after 8 h of annealing. In summary, comparison of the SAXS patterns with the rheology trace suggests that the o-C → G transition at 69 °C (ΔT = 5 °C) is a one-step nucleation and growth process, with a substantial induction time. A particular description of the nucleation process has been proposed.[8]

Figure 4b represents the modulus and SAXS patterns recorded following a deeper temperature quench (ΔT = 14 °C). The initial o-C phase was attained at 90 °C, as indicated by a two-spot reflection pattern (not shown) similar to pattern (1) in Figure 4a. Following the temperature quench to 60 °C, four off-equator spots (at ±50° relative to the equator) emerge very quickly and intensify with time (patterns (1) and (2) in Figure 4b). However, these four off-equator reflections then decline in intensity and eventually disappear,[30] while the characteristic 10-spot gyroid pattern emerges and increases in intensity at long annealing times (pattern (3) in Figure 4b). From the comparison of these SAXS patterns and the rheology trace, the o-C → G transition following deep quenches was confirmed to occur via two distinct stages. The initial step is the formation of an intermediate structure, which also corresponds to the first step increase observed in G'. The growth of the intermediate structure results in a slight increase in G' at the first plateau (pattern (2) in Figure 4b). Subsequently, the gyroid structure starts to grow from the intermediate state (pattern (3) in Figure 4b) and contributes to the second, major increase in G'. The reflection spots associated with G continued to sharpen slightly even after 48 h of annealing, implying that the G structure develops full long-range order very slowly, as suggested by the failure to achieve the second plateau in G'. The crossover temperature at which the transition mechanism changes from a one-step to a two-step process involving an intermediate state is denoted as T_x and is approximately located at 68 °C (ΔT = 6 °C) as marked in Figure 2.

Intermediate State. The SAXS pattern (2) in Figure 4b exhibits scattering features consistent with a hexagonally perforated layer structure (HPL).[28,39] At the equator, the peak positions of the strong reflections and weak higher-order reflections are in the ratio of 1:2 (q^* and $2q^*$). These reflections indicate that this intermediate phase exhibits a layerlike structure with layers parallel to the (10) planes of the initial oriented cylinder phase. In addition to the four intense off-equator reflections (at 50 ± 3° relative to the equator and at q = $0.95q^*$), four very weak higher-order reflections at 28 ± 3° with respect to the equator and at q = $1.65q^*$ characterize the stacking of the in-plane perforations (these reflections are not readily discerned in pattern 2). In the HPL structure, the majority component (PI in this case) penetrates through the minority component layers (PS) via hexagonally arranged channels, which connect the layers formed by the majority component. Hence, the HPL structure can be modeled as staggered layers comprising hexagonal perforations. The SAXS patterns can then be interpreted as resulting from an ABCABC... stacking of perforated planes[39] or a combination of ABCABC... and ABAB... stacking.[28] The HPL structure has been reported as an intermediate metastable phase between L and C[40,41] and is predicted theoretically to be a kinetic pathway for the L → C transition.[6,42] The HPL structure has also been identified as a long-lived nonequilibrium state,[43−47] which can facilitate the L → G transition.[24] It should be noted that the evidence presented here is not conclusive for the assignment of the intermediate phase as HPL, and more detailed characterization of the intermediate structure would be desirable. This exposes two disadvantages of employing solutions for this kind of work: the difficulty in performing electron microscopy and the difficulty in removing oriented samples for scattering analysis along other directions.

Transition Epitaxy. In pattern (3) of Figure 4a, the 10 intense reflections, two at the equator, four at ±28°, and four at ±70° with respect to the equator, can be indexed as reflections from {211} planes of the gyroid cubic lattice, and the four very weak second-order spots at ±60° relative to the equator are consistent with reflections from {220} planes, as described in detail by previous workers.[28,38] The presence of these reflections suggests that the gyroid phase is a directionally oriented polycrystal, comprising grains with the [111] axis coinciding with the shear direction (z axis), but with various orientations of the {211} and {220} planes that intersect with the [111] direction. In particular, the retention of the equatorial spots through the transition indicates that the gyroid phase transforms from the o-C phase with the following epitaxial relationship: C (10) → G (211). This epitaxial transition from C → G was first demonstrated in nonionic surfactant/water systems[48,49] and later shown in block copolymer mixtures.[27,28] This epitaxy has also been anticipated theoretically.[8]

In Figure 4b, the equatorial spots persist through the transformation of o-C → HPL (patterns (1) and (2)) and the conversion of G from HPL (pattern (3)). These results indicate that both steps proceed epitaxially in

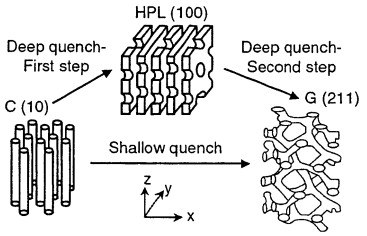

Figure 5. Epitaxial relationships among C, G, and HPL phases.

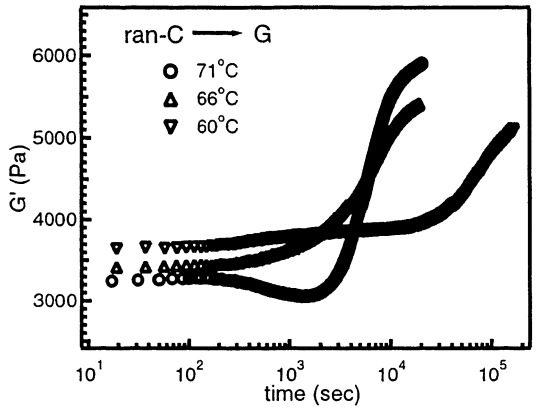

Figure 6. Evolution of G' ($\gamma = 1\%$ and $\omega = 1$ rad/s) following quenches from ran-C to the indicated temperatures.

the two-stage mechanism for the o-C → G transition. The epitaxy of the HPL → G transition in block copolymers has been established.[43−45] The epitaxial relationships among these microstructures, C (10) → HPL (100), HPL (100) → G (211), and C (10) → G (211), are illustrated in Figure 5. The epitaxially related lattice planes, C(10), HPL(100), and G(211), are projected along the $y-z$ plane in these 3D pictures, and the X-ray beam is incident along the y axis. Moreover, Figure 5 emphasizes that different transition mechanisms are observed for various quench depths. A single step transformation takes place at shallow quenches ($\Delta T < 6$ °C), whereas two distinct stages are established for the o-C → G transition following deep quenches ($\Delta T > 6$ °C).

The ran-C → G Transition. The solution was first heated to the disordered state to eliminate all thermal history, and then annealed at 85 °C, forming a randomly oriented cylinder phase. The ran-C phase was quenched to various lower temperatures, and G' was measured vs time, as shown in Figure 6. For the quench temperature of 71 °C, G' decreased slightly near 10^3 s, possibly due to partial alignment of the cylinders. Nevertheless, G' increased predominantly in one step following different temperature quenches, and the apparent induction time became extremely long at deep quenches, e.g., 2×10^4 s at 60 °C.

The 2D SAXS images of the randomly oriented microstructures exhibited concentric rings of intensity. To elucidate the evolution with time, these images were azimuthally averaged to the 1D form of intensity vs the scattering vector q. Representative 1D SAXS profiles for the ran-C → G transition at 63 °C are displayed in Figure 7. Curve 1 attained at 85 °C shows the characteristic scattering of the hexagonally packed cylindrical microstructure; the primary peak and the weak second-order peak are in the position ratio $1:\sqrt{3}$. The absence of other higher-order peaks is attributable to the proximity of the annealing temperature (85 °C) to T_{ODT} (122 °C); i.e., the system is relatively weakly segregated.

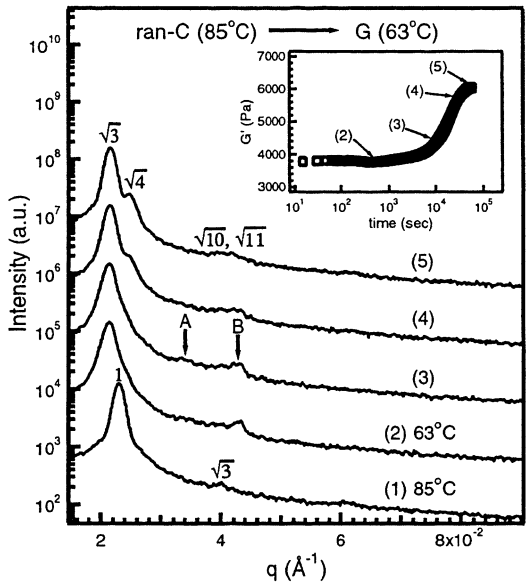

Figure 7. Evolution of isotropic SAXS intensities following a quench from ran-C to G at 63 °C. The curves are matched with the evolution of G' in the inset.

Following the temperature quench to 63 °C, SAXS patterns were collected over time, and some of the 1D profiles are shown, with the intensity shifted vertically for clarity. In less than 10 min after the sample holder reached the quench temperature, the position of the primary peak q^* moved to a distinctly smaller value, and two weak higher-order peaks (marked as A and B) appeared and grew slightly with time, as curves 2 (10 min) and 3 (3 h) show. However, no significant change was observed in the elastic modulus G' over the same interval (see the inset). At long annealing times, peaks A and B disappeared, and the characteristic reflections of the G structure (peak position ratio $\sqrt{3}:\sqrt{4}:\sqrt{10}:\sqrt{11}$) emerged and sharpened with time, as illustrated by curves 4 and 5 obtained at 9 and 15 h, respectively. As indicated in the inset, the growth of G accounts for the significant increase in G' at long annealing times.

Transient scattering profiles similar to curves 2 and 3 were also observed during other deep quench experiments from the ran-C phase ($\Delta T > 6$ °C). The positions of the weak higher-order peaks located at 1.65 q^* (peak A) and $2q^*$ (peak B) are consistent with those of higher-order spots characterizing the HPL structure (i.e., pattern (2) in Figure 4b). Accordingly, these results indicate that ran-C → G also proceeds via two steps following deep quenches and that the HPL structure appears as an intermediate state. Relative to the o-C structure, HPL has the larger elastic modulus due to the connectivity between the layers. However, ran-C also has a larger modulus than o-C, due to the random orientation and entanglement of the cylinders. Thus, coincidentally, the elastic modulus of the HPL structure is comparable to that of the ran-C phase such that the rheology traces in Figure 6 appear to exhibit an anomalously long induction period during the first stage of transition (ran-C to HPL). Hence, the time evolution of G' only reveals the second step of the transition, i.e., HPL → G. Most importantly, the SAXS results indicate that following deep quenches the ran-C → G transition goes through a similar pathway as the o-C → G transition.

Following shallow quenches from ran-C ($\Delta T < 6$ °C), the characteristic reflections of G were observed to

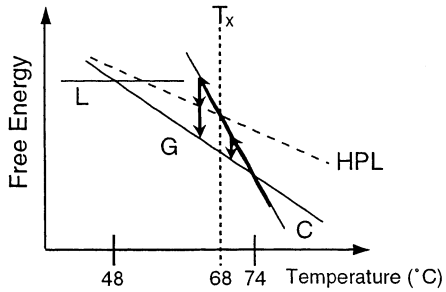

Figure 8. Schematic illustration of the relative free energies of the various states and the transition temperature T_x between shallow and deep quenches.

emerge and intensify with time. No other transient scattering patterns were discernible in the interim. Hence, the transition of ran-C → G appears to be a one-step process for shallow quenches, which is also in accordance with the observation for the o-C → G transition. Therefore, we conclude that the preorientation of the cylinder phase does not affect the C → G transition mechanism in any significant way.

Transition Scenario. The quench temperatures approach the G/L coexistence boundary ($T_{OOT} = 48 \pm 3$ °C) in deep quench experiments. As a result, the free energy of the HPL structure should be very close to that of G at lower quench temperatures.[42,50] Recall that HPL is predicted to have a higher free energy than the lower of either L or G, but to be lower than L over most of the regime where G is the stable phase. The free energy of various microstructures is plotted schematically as a function of temperature in Figure 8, and the arrows indicate the proposed transformation routes. At higher quench temperatures ($T > T_x$), HPL possesses a free energy greater than C and G such that the supercooled C can transform to G directly. On the other hand, following deep quenches, HPL can emerge before G as the free energy of HPL is intermediate to that of C and G (see the dotted line in Figure 8). The observation that HPL develops before G also implies that the energy barrier is smaller for C → HPL than for C → G. It has been proposed that the layerlike structure is formed first to reduce the interfacial tension, which converts to the G structure eventually to relieve the chain packing frustration.[51] The conversion of the intermediate HPL structure to G is very slow, as shown in previous cases for the L → HPL → G sequence.[26,28,52] It should be reiterated that the transformation processes, and this scenario, are equivalent for the o-C → G and ran-C → G transitions. Another possibility to be considered is that T_x corresponds to a stability limit and thus leads to a change in transition mechanism. However, the estimated chain diffusivity for this system ($>10^{-10}$ cm^2/s) implies a time scale of milliseconds for reorganization at the structural length scale (q^*), which is still orders of magnitude faster than the growth of HPL from C.

Following shallow quenches the primary peak position in G deviates slightly from the value extrapolated from the peak positions determined at higher temperatures in C, e.g., $q^* = 0.0222$ Å^{-1} at $T = 69$ °C compared to an extrapolated value of 0.0226 Å^{-1}. This comparison indicates that the lattice spacing persists when G evolves from the slightly supercooled C. Therefore, these results suggest that the C → G transition following a shallow quench can proceed directly and epitaxially via a nucleation and growth mechanism, consistent with the theoretical prediction.[8] However, as will be discussed

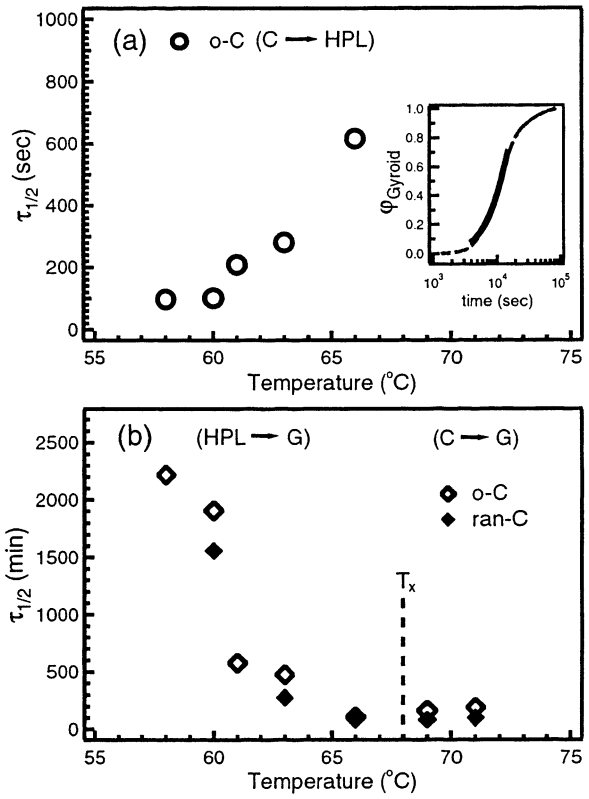

Figure 9. Half-times for the various transitions vs quench temperature (a) for o-C → HPL and (b) for HPL → G and for C → G. Inset in (a) shows the Avrami fit to the quench from o-C to G at 71 °C.

below, it is possible that the 2% mismatch in q^* does result in a subtle distortion to the G structure that persists for long times.

Transition Kinetics. The time evolution of the elastic modulus G', as shown in Figures 3 and 6, exhibits an appoximately sigmoidal shape and was further analyzed using the conventional Avrami functional form. During a transformation from phase A to phase B, it is assumed that the sample comprises only two components, the newly formed phase B dispersed in the original phase A, and that the modulus is a linear combination of the moduli of these two constituent phases. The volume fraction of the new phase φ_B can thus be extracted from the following expression:

$$G' = \varphi_A G'_A + \varphi_B G'_B \tag{4}$$

where $\varphi_A + \varphi_B = 1$. The time dependence of the volume fraction φ_B is then fitted to the Avrami equation:

$$\varphi_B(t) = 1 - \exp(-kt^n) \tag{5}$$

where k is the rate constant and n is the Avrami exponent. The characteristic time scale for the transformation process, the half-time $\tau_{1/2}$, can be calculated from the fit as $(\ln 2/k)^{1/n}$. The inset to Figure 9a provides an example of this analysis for the o-C → G transition at the quench temperature of 71 °C. At this temperature, as shown in Figure 3, only one step increase in G' was observed, which corresponds to the direct transformation o-C → G. Therefore, the original phase was o-C, and G'_{o-C} was taken as the modulus measured immediately after the rheometer reached temperature equilibrium, i.e., the first point on the 71 °C trace in

Table 1. Avrami Half-Times and Exponents for the Various Transitions

		o-C		ran-C	
transition	T, °C	$\tau_{1/2}$ (min)	n	$\tau_{1/2}$ (min)	n
C → G	71	189	2.0	99	2.3
	69	160	1.6	81	2.1
C → HPL	66	10.3	1.2		
	63	4.68	1.5		
	61	3.48	1.5		
	60	1.68	0.9		
	58	1.62	1.0		
HPL → G	66	108	1.5	83	1.3
	63	476	2.0	277	1.7
	61	578	1.6		
	60	1910	1.6	1560	1.0
	58	2220	1.7		

Figure 3. The volume fraction of the G phase, φ_{gyroid}, plotted in the inset was estimated utilizing eq 4, taking the modulus attained at long annealing times as G'_{gyroid}. Equation 5 with $n = 2$ fitted the data reasonably well within the φ_{gyroid} range of 0.1−0.7, and $\tau_{1/2}$ was determined to be 1.1×10^4 s.

For deep quenches from the o-C phase, the elastic modulus G' increased with time in two distinct stages (see Figure 3), and each could be analyzed in a similar manner. As the first stage is assigned to the development of HPL from o-C, the modulus at the first plateau was assumed to be that of the new HPL phase, G'_{HPL}. For instance, G' remains around 3000 Pa (G'_{HPL}) for 3 h at the quench temperature of 60 °C after it quickly increased from 2000 Pa (G'_{o-C}) to near 3000 Pa within the first 10 min. The time dependence of the HPL volume fraction was then estimated based on eq 4 and fitted with eq 5. The half-time $\tau_{1/2}$ for the transformation of o-C to HPL at quench temperatures from 58 to 66 °C was calculated from the fitting parameters and plotted in Figure 9a. The exponent n was about 1−1.5 for these quench temperatures; the various fit parameters are listed in Table 1. The o-C → HPL transformation accelerates at lower quench temperatures, when the free energy difference between these two phases is greater (see Figure 8). As a result, this implies that any associated barrier to the transport of polymer chains is relatively small, and the thermodynamic driving force controls these transition kinetics, via a nucleation and growth process.

The kinetics of the second stage, the transformation of HPL to G, was examined by applying the similar approach, taking the first plateau value as G'_{HPL} and estimating the final modulus at long annealing times as G'_{gyroid}. The half-time $\tau_{1/2}$ of HPL → G at various quench temperatures is plotted in Figure 9b, in this case with $n \approx 1.5-2$. Interestingly, this stage exhibits the opposite temperature dependence, slowing with decreasing quench temperature. As sketched in Figure 8, the free energy of the HPL phase is closer to that of G at lower temperatures, and hence the free energy difference and thermodynamic driving force are smaller. (This inference is based on the observation that the L/G and L/HPL boundaries are nearly indistinguishable.[24]) The slow evolution of HPL → G has been well documented in previous studies involving the L → G transformation. Although the chain dynamics become slower at lower temperatures and might further prolong the transformation at deeper quenches, the data in Figure 9a over the same temperature range suggest that chain dynamics is not a significant factor. Furthermore, the solutions are well above the glass transition temperature for the solvated PS domains (estimated to be below 0 °C). Consequently, the slow kinetics reflect a significant barrier to the transformation, as proposed previously. Figure 9b also includes the half-time $\tau_{1/2}$ obtained at quench temperatures of 69 and 71 °C ($n \approx 1.6-2$), where the elastic modulus G' was observed to increase in one step, corresponding to the direct transition from o-C to G.

The transition kinetics for ran-C → G were analyzed similarly, and the fitting results are also displayed in Figure 9b. For deep quenches the elastic moduli of the ran-C phase and the intermediate HPL phase were comparable (see Figure 6), so that only the slow stage associated with HPL → G could be investigated. The half-time $\tau_{1/2}$ ($n \approx 1-1.7$) at final temperatures from 60 to 66 °C exhibits the same temperature dependence as those attained for the second stage in the o-C → G transition. At higher quench temperatures (69 and 71 °C), the kinetics of the direct ran-C → G transition ($n \approx 2.1-2.3$) also follows the same trend as for o-C → G. Therefore, these results further confirm that the C → G transition mechanisms are essentially identical for well-aligned and randomly oriented cylinders. This conclusion may be contrasted with that of Krishnamoorti and co-workers,[18] who reported in their studies of the C → S transition that the kinetics are much more rapid when the initial cylinder phase was shear-aligned. In their case the formation of S from ran-C produces an essentially disordered array of spheres, and the kinetics of adopting a clear bcc lattice are known to be very slow.[53] Conversely, o-C → S is a rapid transition which prepares the spheres in an array that is much closer to bcc.[15,16] In our case even o-C → G is slow, due in part to the long times needed to nucleate the G phase (for shallow quenches), and apparently it is not appreciably easier or harder to nucleate G from ran-C. Similarly, for deeper quenches where HPL intervenes, the development of HPL from either ran-C or o-C is relatively facile, and the much slower step of HPL → G is not particularly sensitive to the presence or absence of long-range order.

Comparison with Previous Studies of C → G. The C → G transition was first studied in a hexaethylene glycol mono-*n*-dodecyl ether ($C_{12}EO_6$)/water mixture.[48,49] For aqueous solutions containing 65 wt % of surfactant $C_{12}EO_6$, a hexagonal cylinder phase was observed at low temperatures, which transformed to the G and L phases, successively, upon heating. Samples were held either in rectangular glass capillary tubes[49] or between two coaxial cylindrical capillary tubes,[48] and the glass surface induced the alignment of the cylinders formed by the surfactant molecules. The epitaxy C(10) ↔ G(211) was observed. Moreover, Clerc and co-workers[54] studied the kinetics of phase transformations in this $C_{12}EO_6$/water system by applying a millisecond infrared laser temperature-jump technique and synchrotron X-ray diffraction with 50 ms time resolution. Samples were heated within 2 ms by the laser, and G was observed to develop directly from C; no intermediate state was reported. The characteristic time of the C → G transition varied from about 1 to 0.1 s, and the fitting Avrami exponent n was around 1. The kinetics accelerated with increasing degree of superheating, i.e., either increasing the initial temperature in the G phase at a given laser energy or increasing the laser energy at a constant initial temperature.

More recently, two groups have reported studies of the kinetics and mechanism of the C → G transition in block copolymer systems. Using time-resolved SAXS and rheology, Floudas et al. investigated a poly(isoprene-*b*-ethylene oxide) diblock copolymer that transformed from crystalline lamellae to C to G upon heating.[29] Following various temperature increases, G was observed to grow from ran-C. The brief appearance of an intermediate plateau in G' was noted, but not investigated further; similarly, SAXS patterns at intermediate times displayed some features not attributable to either C or G. Consequently, it is possible that these were signatures of an intermediate HPL state, which could not be resolved due to the more rapid kinetics in their system. The transition kinetics were also analyzed on the basis of the Avrami function, and the exponent n was found to be around 2. This was attributed to either two-dimensional growth from heterogeneous nuclei or one-dimensional growth from homogeneous nuclei.[29] For all the transformation processes examined in this work, the fits to eq 5 were adequate if not compelling, and the exponents were rather scattered, largely independent of whether the initial state was ran-C, o-C, or HPL. Consequently, we are hesitant to interpret these exponents in terms of the dimensionality of the growth process.

Vigild et al. investigated order−order transitions in poly((ethylene-*alt*-propylene)-*b*-(dimethylsiloxane)) diblock copolymers via SANS, SAXS, and rheology.[28] The following sequence of phases was identified upon heating a blend consisting of two PEP−PDMS diblock copolymers with slightly different block compositions: L → HPL → G → C → D. The HPL phase was shown to be metastable; e.g., it transformed to G in ca. 3 h at 40 °C and ca. 3 months at room temperature. The C phase was shear-aligned, and G was observed to emerge epitaxially in two stages. The first stage was assigned to the formation of G and the second stage to the perfection of the long-range order. The absence of an intermediate HPL structure in that case might be attributable to a greater difference between the quench temperature and the upper limit of the stable L (68 deg), and thus the crossover temperature T_x was not within the experimentally studied range. In contrast, these two temperatures are less than 20 deg apart in the deep quench experiments reported here. The two stages in the work of Vigild et al.[28] resemble the steep rise and slow saturation of G' reported here, i.e., what we have considered as a single, second stage.

Conservation of Initial Cylinder Orientation during G → C. At the end of a temperature quench experiment, the G phase prepared from either o-C or ran-C was gradually heated back to the C window. The SAXS patterns characteristic of C were recovered, and hence the transitions between C and G were confirmed to be thermoreversible. Figure 10a−c illustrates the SAXS patterns of a particular o-C → G → C cycle. Figure 10a is the scattering pattern of the original o-C, whereas Figure 10b shows the 10-spot G pattern collected after annealing for 13 h following a temperature quench to 66 °C. (Note that the relative brightness of the equatorial spots in Figure 10b is due to the directionally oriented polycrystal of G, not to residual C.) Interestingly, following slow heating (1 °C/min) to 100 °C, a two-spot pattern indicative of a cylinder structure oriented along the shear (z) direction was observed (Figure 10c). As discussed before, the retention of the two bright

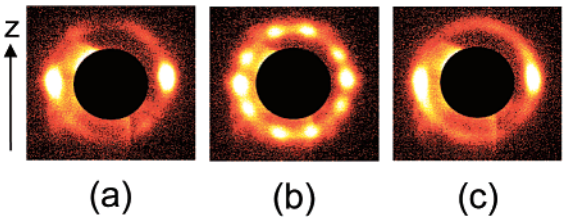

Figure 10. SAXS patterns for (a) initial o-C at 90 °C, (b) G, 13 h after a quench to 66 °C, and (c) after slow heating to 100 °C, showing recovery of initial C orientation.

equatorial spots through the o-C → G transition indicates that the [111] direction of the gyroid lattice lies along the cylinder axis, which in turn is parallel to the z direction. The persistence of the two spots indicates that the cylinders grow back preferentially along the z direction. This result suggests that the reverse transition proceeds epitaxially, G (211) → C (10), which is neither surprising nor a new result. However, there are four nominally equivalent [111] directions for a single crystal of G and presumably even more possible cylinder axes in our sample. Consequently, there is some mechanism by which the G structure "remembers" the C phase from which it evolved. We repeated the cycle, with annealing times in G of 19 and 48 h. In the former case, the result was equivalent to that shown in Figure 10, whereas with the longer annealing the preservation of the original C orientation was noticeably reduced (but not eliminated). Therefore, the origin(s) of this "memory effect" must be very long-lived.

Possibly similar "memory effects" have been reported in the C → S → C transition by Koppi et al.,[11] by Kimishima et al.,[55] and most recently by Lee et al.[19] In the first instance, a shear-oriented PEP−PEE sample was not annealed in the S state, and so the result that the C orientation was recovered is less surprising.[11] Kimishima et al. studied the transitions between C and S in a poly(styrene-*b*-isoprene) melt using SAXS and polarized optical microscopy.[55] The original orientation of the cylinders within a single grain was observed to be recovered after the reverse S → C transition, even after annealing in S for more than 2 h. These authors proposed that the translational diffusion of the chemical junctions connecting two blocks is very slow along the interface, which might result in a nonequilibrium distribution of these junctions.[55] The deficiency in the number density of junctions in some parts of the microdomains could provide a memory for the conservation of the structural orientation. However, measurements of the diffusion of styrene−isoprene copolymers along a lamellar interface have been reported,[56] with which permits an order of magnitude estimate of $D \approx 10^{-12}$ cm^2/s for the relevant molecular weight and temperature. Taking the experimental value of $q^* \approx 0.25$ nm^{-1}, a diffusional relaxation time of $(q^{*2}D)^{-1} \approx 0.1$ s is obtained. This is several orders of magnitude shorter than the reported annealing time, and consequently short-range diffusional limitations do not seem to be the likely explanation. Similarly, in our solutions the diffusion time would be even shorter, whereas the memory is even longer. Lee et al.[19] recently reported a detailed study of the persistence of orientation during multiple C → S → C cycles, and annealing times in excess of 10 h in S were not sufficient to eliminate the memory effect. These authors did not propose an explanation, however.

It seems clear that the memory effect must reflect a subtle nonequilibrium structural feature in the epitaxially grown phase, S or G in the reported cases. This might arise from a small mismatch between the q^* values of the two structures, as noted by Matsen.[9] For example, in C → S the spheres are formed by the cylinders pinching off. In this process the sphere spacing along the *C* axis could correspond exactly to the q^* favored by S, whereas the sphere-to-sphere distance in other directions would be set by the q^* of C. That it can take extremely long times to fully anneal the S phase is well established, and so it is plausible that it might take many hours to erase the memory of the slight lattice mismatch. It is also plausible that a similar explanation could be invoked for the G phase, although the structural details are not easily pictured. An alternative hypothesis is that the reverse transition is preferentially nucleated by grain boundaries and defects, which could have been formed with some memory of the initial state. However, the similarity of the memory effect between macroscopically aligned samples[19] and smaller grains[55] may argue against a dominant role for grain boundaries. Finally, it should be noted that the various crystalline orientations in the G structure that emerge from preoriented C do share a common [111] axis. Consequently, even if the selection of the cylinder axis was a purely statistical process, one would expect to see a preference for the original direction. Whether this is enough to explain the preference exhibited in Figure 10 remains to be established, but it certainly is an issue that merits further attention.

Summary

The kinetics and mechanisms of the C → G transition in a concentrated copolymer solution have been studied using rheology and SAXS. Highly oriented C phases (o-C) were prepared by shear orientation and randomly oriented C phases (ran-C) by quenching from disorder. The o-C → G transition was investigated following temperature quenches into the G window. Comparison of the time evolution of the elastic modulus and 2-dimensional SAXS patterns shows that the transition mechanism changes with quench depth. Following a shallow quench, the supercooled o-C was observed to transform to G epitaxially and directly. In contrast, a two-stage, epitaxial transition mechanism is established for deep quenches, and the SAXS signatures of the intermediate state are consistent with a hexagonally perforated layer structure (HPL). The transition mechanisms and kinetics are similar for the transformation of G from ran-C, and thus the preorientation of the initial C phase does not affect the transition mechanism. The temperature dependence of the transition kinetics was examined based on the time evolution of the elastic modulus. Following deep quenches, the kinetics of C → HPL accelerates with decreasing temperature, in contrast to the temperature dependence of the kinetics of the second step (HPL → G). Thermoreversibility of the transition between C and G was confirmed, and the initial cylinder orientation was observed to be preserved to some extent even after annealing in G for up to 48 h.

Acknowledgment. This work was supported in part by the IPRIME program at the University of Minnesota, the Dupont Analytical group, and the National Science Foundation through Award DMR-9901087. The assistance of K. J. Hanley in sample preparation and helpful discussions with X. Wang and T. Harada are appreciated.

References and Notes

(1) Hamley, I. W. *The Physics of Block Copolymers*; Oxford University Press: Oxford, 1998.
(2) Bates, F. S.; Fredrickson, G. H. *Annu. Rev. Phys. Chem.* **1990**, *41*, 525.
(3) Laradji, M.; Shi, A.-C.; Noolandi, J.; Desai, R. C. *Macromolecules* **1997**, *30*, 3242.
(4) Qi, S.; Wang, Z.-G. *Polymer* **1998**, *39*, 4639.
(5) Qi, S.; Wang, Z.-G. *Phys. Rev. Lett.* **1996**, *76*, 1679.
(6) Qi, S.; Wang, Z.-G. *Phys. Rev. E* **1997**, *55*, 1682.
(7) Goveas, J. L.; Milner, S. T. *Macromolecules* **1997**, *30*, 2605.
(8) Matsen, M. W. *Phys. Rev. Lett.* **1998**, *80*, 4470.
(9) Matsen, M. W. *J. Chem. Phys.* **2001**, *114*, 8165.
(10) Sakurai, S.; Kawada, H.; Hashimoto, T.; Fetters, L. J. *Macromolecules* **1993**, *26*, 5796.
(11) Koppi, K. A.; Tirrell, M.; Bates, F. S.; Almdal, K.; Mortensen, K. *J. Rheol.* **1994**, *38*, 999.
(12) Sakurai, S.; Hashimoto, T.; Fetters, L. J. *Macromolecules* **1996**, *29*, 740.
(13) Kim, J. K.; Lee, H. H.; Ree, M.; Lee, K.-B.; Park, Y. *Macromol. Chem. Phys.* **1998**, *199*, 641.
(14) Ryu, C. Y.; Lee, M. S.; Hajduk, D. A.; Lodge, T. P. *J. Polym. Sci., Polym. Phys. Ed.* **1997**, *35*, 2811.
(15) Ryu, C. Y.; Vigild, M. E.; Lodge, T. P. *Phys. Rev. Lett.* **1998**, *81*, 5354.
(16) Ryu, C. Y.; Lodge, T. P. *Macromolecules* **1999**, *32*, 7190.
(17) Krishnamoorti, R.; Silva, A. S.; Modi, M. A.; Hammouda, B. *Macromolecules* **2000**, *33*, 3803.
(18) Krishnamoorti, R.; Modi, M. A.; Tse, M. F.; Wang, H.-C. *Macromolecules* **2000**, *33*, 3810.
(19) Lee, H. H.; Jeong, W.-Y.; Kim, J. K.; Ihn, K. J.; Kornfield, J. A.; Wang, Z.-G.; Qi, S. *Macromolecules* **2002**, *35*, 785.
(20) Sakurai, S.; Momii, T.; Taie, K.; Shibayama, M.; Nomura, S. *Macromolecules* **1993**, *26*, 485.
(21) Sakurai, S.; Umeda, H.; Taie, K.; Nomura, S. *J. Chem. Phys.* **1996**, *105*, 8902.
(22) Hajduk, D. A.; Gruner, S. M.; Rangarajan, P.; Register, R. A.; Fetters, L. J.; Honeker, C.; Albalak, R. J.; Thomas, E. L. *Macromolecules* **1994**, *27*, 490.
(23) Hajduk, D. A.; Takenouchi, H.; Hillmyer, M. A.; Bates, F. S.; Vigild, M. E.; Almdal, K. *Macromolecules* **1997**, *30*, 3788.
(24) Hajduk, D. A.; Ho, R. M.; Hillmyer, M. A.; Bates, F. S.; Almdal, K. *J. Phys. Chem. B* **1998**, *102*, 1356.
(25) Sakurai, S.; Umeda, H.; Furukawa, C.; Irie, H.; Nomura, S.; Lee, H. H.; Kim, J. K. *J. Chem. Phys.* **1998**, *108*, 4333.
(26) Hamley, I. W.; Fairclough, J. P. A.; Ryan, A. J.; Mai, S.-M.; Booth, C. *Phys. Chem. Chem. Phys.* **1999**, *1*, 2097.
(27) Schulz, M. F.; Bates, F. S.; Almdal, K.; Mortensen, K. *Phys. Rev. Lett.* **1994**, *73*, 86.
(28) Vigild, M. E.; Almdal, K.; Mortensen, K.; Hamley, I. W.; Fairclough, J. P. A.; Ryan, A. J. *Macromolecules* **1998**, *31*, 5702.
(29) Floudas, G.; Ulrich, R.; Wiesner, U. *J. Chem. Phys.* **1999**, *110*, 652.
(30) Wang, C.-Y.; Lodge, T. P. *Macromol. Rapid Commun.* **2002**, *18*, 49.
(31) Hanley, K. J.; Lodge, T. P. *J. Polym. Sci., Polym. Phys. Ed.* **1998**, *36*, 3101.
(32) Hanley, K. J.; Lodge, T. P.; Huang, C.-I. *Macromolecules* **2000**, *33*, 5918.
(33) Hanley, K. J. Block Copolymers: Phase Behavior in Neutral and Selective Solvents. Ph.D. Thesis, University of Minnesota, 2001.
(34) Lodge, T. P.; Pudil, B.; Hanley, K. J. *Macromolecules* **2002**, *35*, 4707.
(35) Lodge, T. P.; Bang, J.; Wang, X. *Phys. Rev. Lett.*, submitted for publication.
(36) Ehlich, D.; Takenaka, M.; Okamoto, S.; Hashimoto, T. *Macromolecules* **1993**, *26*, 189.
(37) de Gennes, P. G. *The Physics of Liquid Crystals*; Oxford University Press: London, 1975.
(38) Hamley, I. W.; Pople, J. A.; Gleeson, A. J.; Komanschek, B. U.; Towns-Andrews, E. *J. Appl. Crystallogr.* **1998**, *31*, 881.
(39) Ahn, J.-H.; Zin, W.-C. *Macromolecules* **2000**, *33*, 641.
(40) Hamley, I. W.; Gehlsen, M. D.; Khandpur, A. K.; Koppi, K. A.; Rosedale, J. H.; Schulz, M. F.; Bates, F. S.; Almdal, K.; Mortensen, K. *J. Phys. II* **1994**, *4*, 2161.

(41) Hamley, I. W.; Koppi, K. A.; Rosedale, J. H.; Bates, F. S.; Almdal, K.; Mortensen, K. *Macromolecules* **1993**, *26*, 5959.
(42) Qi, S.; Wang, Z.-G. *Macromolecules* **1997**, *30*, 4491.
(43) Förster, S.; Khandpur, A. K.; Zhao, J.; Bates, F. S.; Hamley, I. W.; Ryan, A. J.; Bras, W. *Macromolecules* **1994**, *27*, 6922.
(44) Khandpur, A. K.; Förster, S.; Bates, F. S.; Hamley, I. W.; Ryan, A. J.; Bras, W.; Almdal, K.; Mortensen, K. *Macromolecules* **1995**, *25*, 8796.
(45) Zhao, J.; Majumdar, B.; Schulz, M. F.; Bates, F. S.; Almdal, K.; Mortensen, K.; Hajduk, D. A.; Gruner, S. M. *Macromolecules* **1996**, *29*, 1204.
(46) Schulz, M. F.; Khandpur, A. K.; Bates, F. S.; Almdal, K.; Mortensen, K.; Hajduk, D. A.; Gruner, S. M. *Macromolecules* **1996**, *29*, 2857.
(47) Almdal, K.; Mortensen, K.; Ryan, A. J.; Bates, F. S. *Macromolecules* **1996**, *29*, 5940.
(48) Rancon, Y.; Charvolin, J. *J. Phys. Chem.* **1988**, *92*, 2646.
(49) Clerc, M.; Levelut, A. M.; Sadoc, J. F. *J. Phys. II* **1991**, *1*, 1263.
(50) Matsen, M. W.; Bates, F. S. *Macromolecules* **1996**, *29*, 1091.
(51) Matsen, M. W.; Bates, F. S. *Macromolecules* **1996**, *29*, 7641.
(52) Hajduk, D. A.; Ho, R.-M.; Hillmyer, M. A.; Bates, F. S.; Almdal, K. *J. Phys. Chem. B* **1998**, *102*, 1356.
(53) LaMonte Adams, J.; Quiram, D. J.; Graessley, W. W.; Register, R. A.; Marchand, G. R. *Macromolecules* **1996**, *29*, 2929.
(54) Clerc, M.; Laggner, P.; Levelut, A.-M.; Rapp, G. *J. Phys. II* **1995**, *5*, 901.
(55) Kimishima, K.; Koga, T.; Hashimoto, T. *Macromolecules* **2000**, *33*, 968.
(56) Hamley, I. W.; Pople, J. A.; Diat, O. *Colloid Polym. Sci.* **1998**, *276*, 446.

MA0205212